Heliyon 10 (2024) e24598

Contents lists available at ScienceDirect

Heliyon

journal homepage: www.cell.com/heliyon

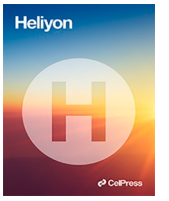

Research article

Advanced glycation end products regulate macrophage apoptosis and influence the healing of diabetic foot wound through miR-361-3p/CSF1R and PI3K/AKT pathway

Yongzhi Jin [a,1], Yi Huang [a,1], Guang Zeng [a], Junsheng Hu [a], Mengfan Li [b], Ming Tian [c,***], Tao Lei [d,**], Rong Huang [a,*]

[a] Department of General Surgery, Putuo Hospital, Shanghai University of Traditional Chinese Medicine, Shanghai, 200062, China
[b] Department of General Surgery, LiQun Hospital, Shanghai, 200333, China
[c] Shanghai Burn Institute, Department of Burn, Ruijin Hospital, Shanghai Jiaotong University School of Medicine, Shanghai, 200025, China
[d] Department of Endocrinology, Putuo Hospital, Shanghai University of Traditional Chinese Medicine, Shanghai, 200062, China

ARTICLE INFO

Keywords:
Diabetic foot ulcer
Crucial feature genes
Macrophages
Wound healing
Advanced glycation end products

ABSTRACT

Background: Diabetic foot ulcers (DFUs) are a severe complication of diabetes. Persistent inflammation and impaired vascularization present considerable challenges in tissue wound healing. The aim of this study was to identify the crucial regulators of DFU wound healing and investigate their specific mechanisms in DFU.

Methods: DFU RNA sequencing data were obtained to identify crucial feature genes. The expression levels of the feature genes and their corresponding microRNAs (miRNAs) were verified in clinical samples. Subsequently, the expression of CD68 was determined in DFU and non-diabetic foot skin samples. RAW 264.7 cells were treated with advanced glycation end products (AGEs) to determine their viability and apoptosis. Finally, the roles of the selected crucial genes and their corresponding miRNAs were investigated using *in vitro* experiments and a mouse model of diabetes.

Results: Bioinformatic analysis showed that five crucial feature genes (*CORO1A*, *CSF1R*, *CTSH*, *NFE2L3*, and *SLC16A10*) were associated with DFU wound healing. The expression validation showed that miR-361-3p-CSF1R had a significant negative correlation and was thus selected for further experiments. AGEs significantly inhibited the viability of RAW 264.7 cells and enhanced their apoptosis; furthermore, the AGEs significantly downregulated CSF1R and increased miR-361-3p levels compared with the control cells. Additionally, inhibition of miR-361-3p decreased the cell apoptosis caused by AGEs and increased the levels of p-AKT/AKT and p-PI3K/PI3K, whereas CSF1R knockdown reversed the effects of miR-361-3p. *In vivo* experiments showed that miR-361-3p inhibition promoted wound healing in diabetic mice and regulated PI3K/AKT levels.

Conclusions: AGEs may regulate macrophage apoptosis via the miR-361-3p/CSF1R axis and PI3K/AKT pathway, thereby influencing DFU wound healing.

* Corresponding author. Department of General Surgery, Putuo Hospital, Shanghai University of Traditional Chinese Medicine, 164 Lanxi Rd, Shanghai, 200062, China.
** Corresponding author.
*** Corresponding author.
E-mail addresses: tianming198@163.com (M. Tian), leitao5899@126.com (T. Lei), huangrongsci@163.com (R. Huang).
[1] Co-first authors.

https://doi.org/10.1016/j.heliyon.2024.e24598
Received 4 September 2023; Received in revised form 3 January 2024; Accepted 10 January 2024
Available online 17 January 2024

1. Introduction

Foot ulcers are one of the most common complications of diabetes and the main cause of lower-extremity amputations. The annual incidence of diabetic foot ulcers (DFUs) worldwide is 6.3%, with North America having the highest prevalence at 13.0% [1]. It is reported that from 1.0 to 3.5 million patients in the US are affected by DFU, and its incidence rate has been estimated to be from 15% to 25% throughout the lifetime of diabetic patients [2]. The risk factors contributing to refractory wounds in DFUs include peripheral vascular disease, neuropathy, poor glycemic control, and infection susceptibility [2]. Most of these factors do not independently cause ulcers. Conventional medical therapy mainly involves the use of chemical drugs and the surgical reconstruction of blood flow. Although considerable progress has been made, the outcomes remain suboptimal worldwide, and a proportion of patients ultimately develop irreversible damage [3]. Thus, there is an urgent need to further explore the pathogenesis of DFU and identify effective therapeutic targets.

Wound healing is a complex process that can be divided into four stages: hemostasis, inflammation, proliferation, and remodeling. Compared with non-diabetic wounds, the inflammatory stage of diabetic wound healing is prolonged, and the inflammatory cytokines such as tumor necrosis factor-α (TNF-α), interleukin (IL)-1β, and IL-6 are oversecreted, which leads to increased tissue damage and delayed diabetic wound healing due to their interference with the proliferation and remodeling stages [4]. Neutrophils, monocytes, and

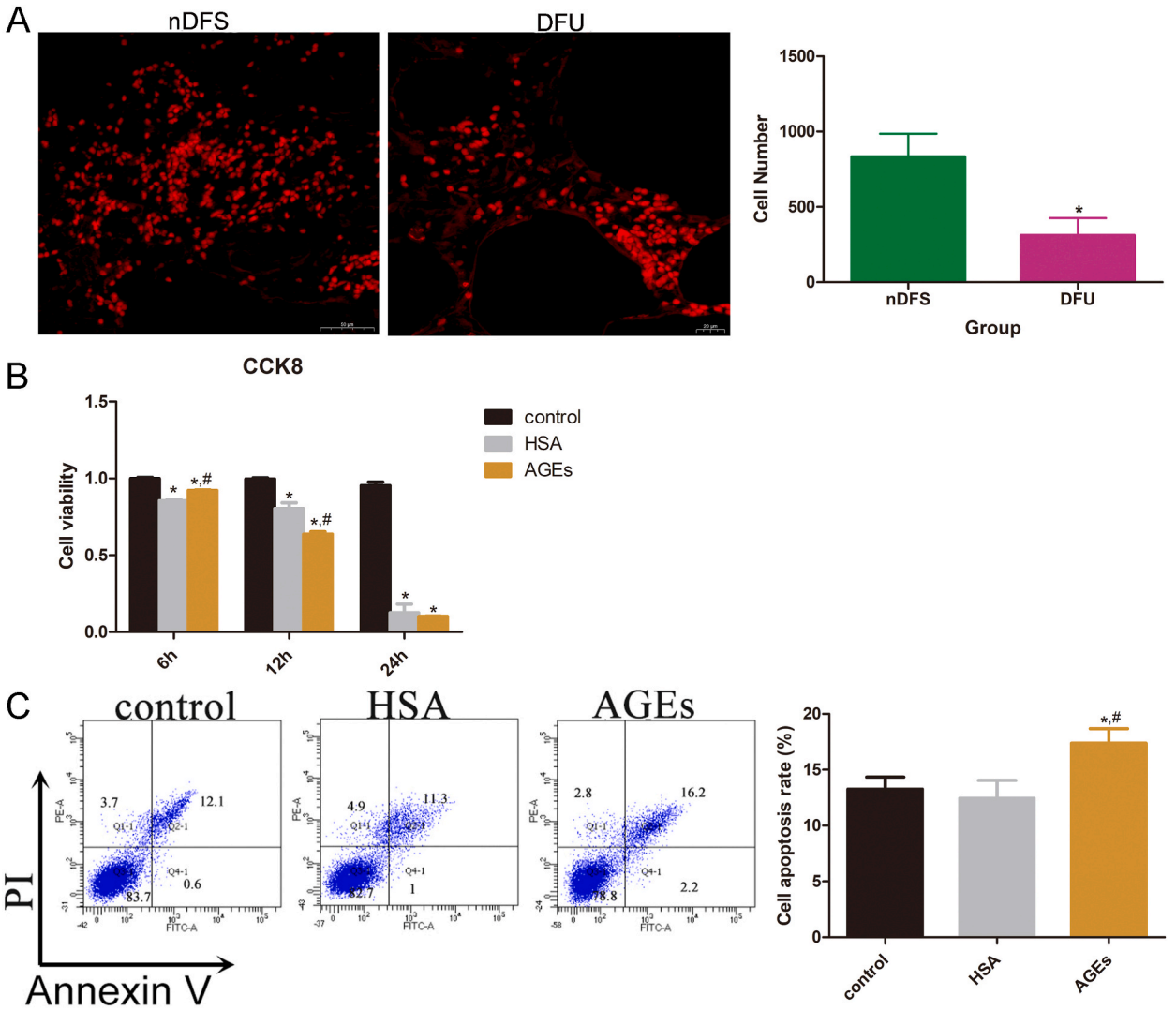

Fig. 1. Advanced glycation end products (AGEs) inhibited viability and enhanced apoptosis of macrophages in diabetic foot ulcer (DFU). (A) Expression of CD68 (macrophage number) in the clinical samples of DFU and non-diabetic foot skin (nDFS). $^{*}P < 0.05$, compared with the nDFS group. (B) Viability of RAW 264.7 cells with different treatments after cultured for 6, 12, and 24 h using cell counting kit-8. (C) Apoptosis of RAW 264.7 cells with different treatments after cultured for 12 h using flow cytometry. $^{*}P < 0.05$, compared with the control group. $^{\#}P < 0.05$, compared with the HAS group.

macrophages are the primary immune cells that cooperate during the onset, progression, and resolution of inflammation [5,6]. Monocytes circulating in the blood are recruited to the inflamed tissues and transformed into macrophages. Exposure to proinflammatory cytokines and microbial products contributes to M1 macrophage activation. During healing, the macrophage population shifts from a predominantly proinflammatory M1 phenotype to an anti-inflammatory M2 phenotype [7]. However, patients with diabetes display higher levels of M1 macrophages than M2 macrophages [8]. Macrophage efferocytosis of apoptotic neutrophils orchestrates the resolution of inflammation by releasing anti-inflammatory molecules [9]. The wounds of diabetic mice show significant impairment in macrophage efferocytosis, which is associated with increased apoptosis of immune cells in damaged tissues [10]. Thus, maintaining a balance between macrophage phenotypes and proper frequency is essential for inflammatory response and wound healing.

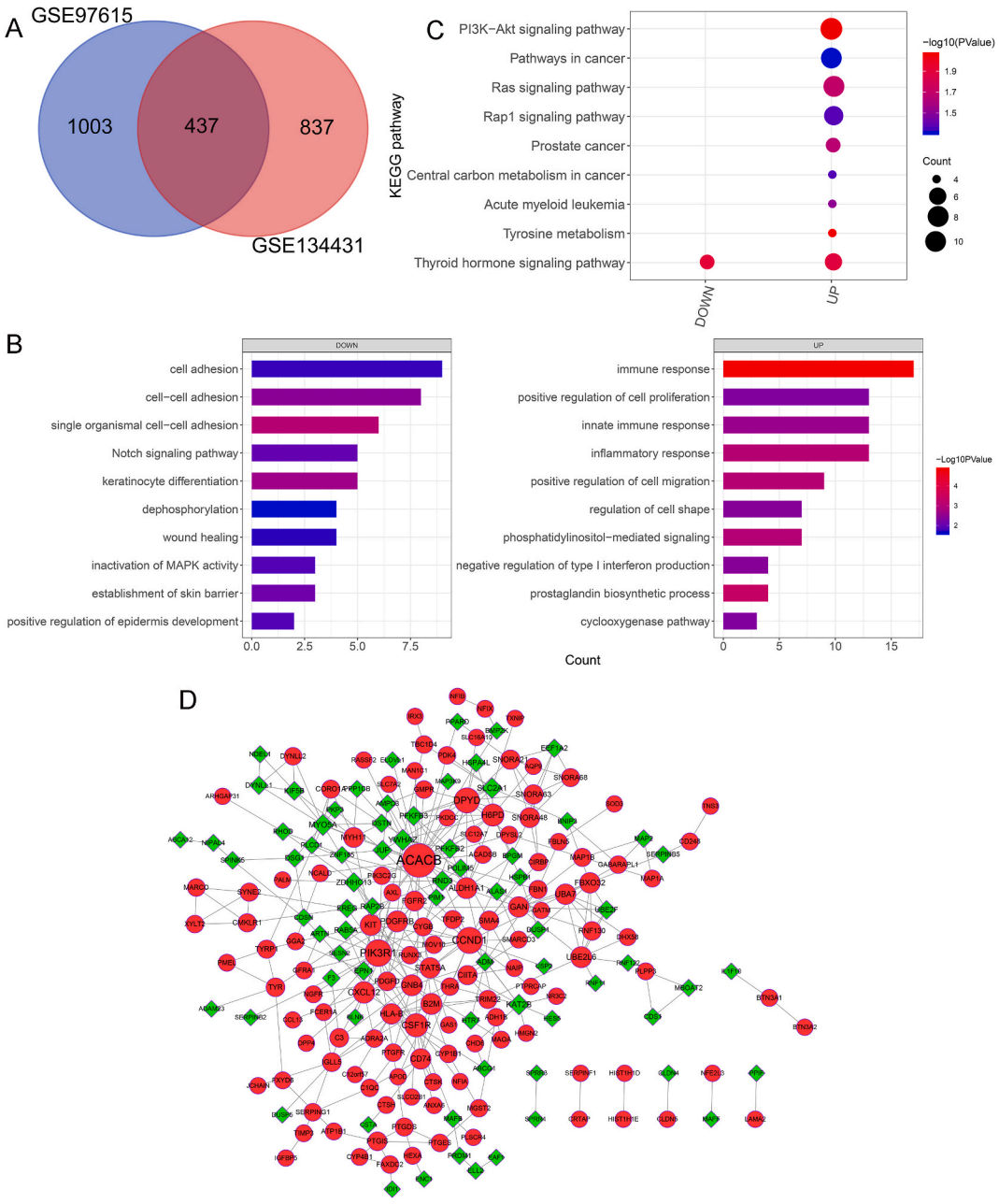

Fig. 2. Identification of the crucial differentially expressed genes (DEGs) related to diabetic wound healing. (A) Venn diagram of DEGs between the DFU and nDFS samples in the GSE134431 and GSE97615 datasets. (B) Top 10 Gene Ontology (GO) terms of biological process enriched by down-regulating trend DEGs (left) and up-regulating trend DEGs (right). (C) Nine significantly enriched Kyoto Encyclopedia of Genes and Genomes (KEGG) pathways of the identified 360 DEGs in the 16 clusters. (D) Construction of a protein-protein interaction network based on the identified 360 DEGs in the 16 clusters.

MicroRNAs (miRNAs) are endogenously expressed non-coding small RNAs that negatively modulate target gene expression by complementary binding to their untranslated regions, resulting in miRNA cleavage or translational silencing [11]. Several miRNAs have been found to regulate the complex biological processes involved in diabetic wound healing. For example, miR-129 and miR-335 promote wound healing by inhibiting Sp1-mediated MMP-9 production, resulting in diabetic keratinocyte migration and skin recovery [12]. Suppression of miR-199a-5p increases the *VEGFA* and *ROCK1* expression levels and promotes impaired wound healing, indicating a therapeutic effect of miR-199a-5p on diabetic wounds [13]. Moreover, high-throughput sequencing of miRNAs in stem cell-derived exosomes revealed higher proportions than that in fibroblast-associated exosomes, and stem cell-derived exosomal miRNAs could lead to a decrease in inflammation, activation of wound cell proliferation, and angiogenesis in mice with diabetic wounds [14]. Zhang et al. [15] reported that macrophages are key players in diabetes complications and that miR-144-5p, an exosomal miRNA from bone marrow-derived macrophages in type 2 diabetes, impairs fracture healing by targeting *Smad1*. These findings suggest that the use of miRNAs may be a promising strategy for improving impaired diabetic wound healing.

In addition, in long-term hyperglycemia, the accumulated advanced glycation end products (AGEs) can increase the secretion of proinflammatory cytokines and production of reactive oxygen species (ROS), which are pivotal signaling molecules that contribute to the progression of inflammatory diseases [16]. The interaction between AGEs and receptors for AGEs (RAGEs) activates Toll-like receptor 4 (TLR4) signaling and promotes macrophage polarization from M0 to M1 [17]. In addition, AGE treatment enhances the generation of proinflammatory cytokines, upregulates the expression of M1 macrophage-associated markers (iNOS and CD11c), and downregulates M2 macrophage-related markers (Arg1 and CD26) through the MAPK pathway, thereby participating in the pathogenesis of diabetes [18]. In patients with DFU, long-term hyperglycemia and high AGE levels contribute to a prolonged inflammatory phase and suboptimal inflammation levels that are insufficient to promote wound healing [19]. Therefore, in this study, AGEs were used to treat macrophages and the role of macrophage apoptosis in DFU was determined. RNA-seq datasets were obtained to comprehensively analyze crucial feature genes associated with DFU would healing. Next, the mechanisms of the selected feature genes and their corresponding crucial miRNAs in DFU wound healing were explored in a cellular experiment and diabetic mouse model. This study enhances our understanding of the basic mechanisms underlying diabetic wound healing and provides potential therapeutic targets for DFU.

2. Results

2.1. AGEs inhibited viability and enhanced apoptosis of macrophages in DFU

The expression of CD68 (a macrophage surface marker) was analyzed to determine the number of macrophages in DFU. The expression of CD68 in DFU tissues was significantly lower than that in the non-diabetic foot skin (nDFS) group ($P < 0.05$, Fig. 1A), indicating that the number of macrophages in DFU was decreased. Therefore, RAW 264.7 cells (macrophages) were selected for further experiments.

Next, the role of AGEs in macrophage viability and apoptosis was determined. After culturing for 6, 12, and 24 h, both HSA and AGE treatments significantly inhibited cell viability compared to the control cells ($P < 0.05$, Fig. 1B). However, when the cells were treated for 6 h, the cell viability in the AGE group was evidently higher than that in the HSA group; and when treated for 12 h, AGE treatment significantly suppressed the viability of RAW 264.7 cells compared with the HSA treatment ($P < 0.05$, Fig. 1B). Therefore, the cells cultured for 12 h were used for subsequent experiments. The results of flow cytometry showed no significant difference in cell apoptosis between the control and HSA-treated cells ($P > 0.05$, Fig. 1C), whereas AGEs treatment significantly increased the apoptosis of RAW 264.7, compared with the control cells ($P < 0.05$, Fig. 1C). These results indicate the importance of macrophage apoptosis in DFU and that AGEs could inhibit cell viability while enhancing the apoptosis of macrophages.

2.2. Identification of the crucial differentially expressed genes (DEGs) related to diabetic wound healing

To further investigate the molecular mechanisms of DFU pathogenesis, bioinformatics analysis was performed on GEO datasets, including GSE134431 and GSE97615. Based on $P < 0.05$ and $|\log_2 FC| > 1$, a total of 1274 and 1440 differentially expressed genes (DEGs) were screened from the GSE134431 and GSE97615 datasets, respectively (Fig. 2A). To identify the crucial genes related to the healing process in DFU and eliminate the interference of normal wound healing, 837 DEGs were selected as specific genes related to the healing process in DFU and used for Mfuzz cluster analysis. In the DFU non-healers, DFU healers, and nDFS groups, 837 DEGs were divided into 16 clusters (Figure S1). Clusters 1, 2, 4, 5, 7, 8, 12, and 13 were up-clustered and contained 217 genes that were upregulated during the healing process, whereas clusters 3, 11, and 14 were down-clustered and contained 143 genes that were downregulated during the healing process.

Subsequently, 217 genes with upregulating trends and 143 genes with downregulating trends were submitted for functional analyses, and it was found that these genes were significantly enriched in 40 Gene Ontology (GO) terms of biological processes and 9 Kyoto Encyclopedia of Genes and Genomes (KEGG) pathways (Fig. 2B and C). The genes with downregulated trends were significantly related to “cell adhesion,” “Notch signaling pathway,” “wounding healing,” “inactivation of MAPK activity,” and “establishment of skin barrier.” Meanwhile, the significantly enriched GO terms of the genes with upregulating trends included “immune response,” “inflammatory response,” “cyclooxygenase pathway,” and “phosphatidylinositol-mediated signaling” (Fig. 2B). The significantly enriched KEGG pathways were shown as follows: “PI3K/Akt pathway,” “thyroid hormone signaling pathway,” “pathways in cancer,” “Ras signaling pathway,” and “Rap1 signaling pathway” (Fig. 2C). In addition, 217 upregulated and 143 downregulated genes were used to construct a protein–protein interaction (PPI) network comprising 201 proteins and 354 edges (Fig. 2D).

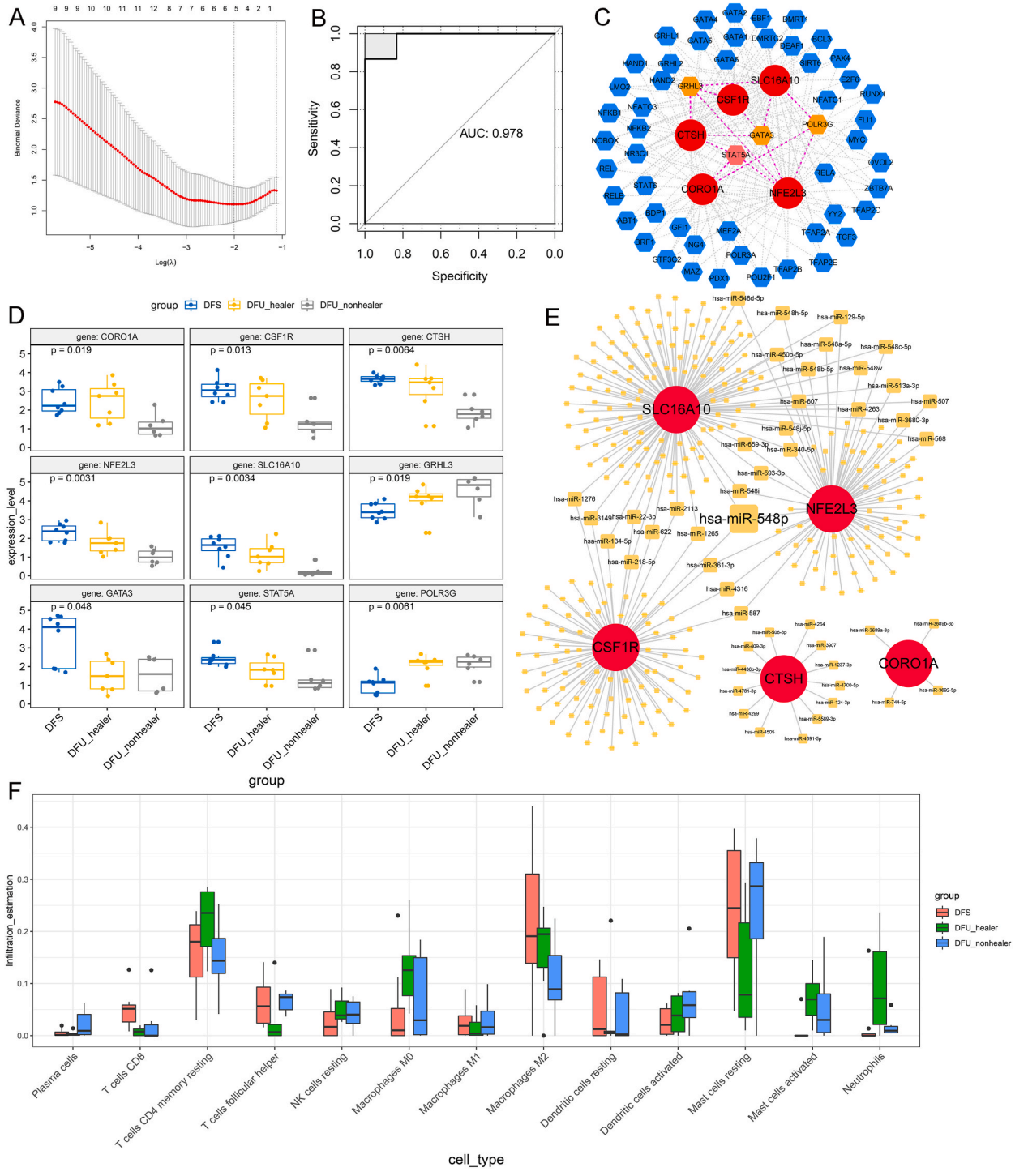

Fig. 3. Selection of crucial feature genes, and prediction of miRNAs and upstream transcription factors (TFs) of the genes. (A) Selection of the tuning parameter "λ" in the LASSO model. (B) ROC curves of diagnostic models based on the obtained five crucial feature genes. (C) TFs regulatory network of the five crucial feature genes. The red circles represent the five feature genes, and the hexagons represent the predicted transcription factors. (D) Expression of the five crucial feature genes and the four TFs in the different groups. (E) Regulatory network of the miRNA-crucial feature genes. (F) Correlation analysis between the five crucial feature genes and immune cell infiltration.

2.3. Selection of crucial feature genes, and prediction of miRNAs and upstream transcription factors (TFs) of the genes

Based on the expression levels of all the genes in the PPI network in the GSE134431 dataset, the LASSO regression model with lambda.min as λ was used to select the optimal DEGs (Fig. 3A), and five crucial feature genes including *CORO1A*, *CSF1R*, *CTSH*, *NFE2L3* and *SLC16A10* were obtained with their corresponding regression coefficients of 0.168, 0.161, 0.302, 0.767, and 0.153, respectively. After calculating the eigenvalue for each sample, a receiver operating characteristic (ROC) curve was generated to verify the diagnostic ability of the feature genes in DFU non-healer and healer/nDFS samples. The area under the curve (AUC) value was 0.978 (>0.95), indicating a highly effective predictive ability of the gene cohorts (Fig. 3B).

Upstream transcription factor (TF) prediction analysis was carried out on these five feature gene proteins. A total of 54 TFs were identified, and 196 TF–target relation pairs were formed (Fig. 3C). It was found that *STAT5A* was a hub node in the network with the highest degree of connectivity (degree = 49), and the expression levels of *GRHL3*, *GATA3*, and *POLR3G* showed significant intergroup variability. Furthermore, five feature genes and four TFs were selected for analysis of their expression in the different groups (Fig. 3D).

Five feature genes were used for miRNA prediction, and 339 miRNA–gene pairs were obtained (Fig. 3E). Notably, hsa-miR-548p targeted three feature genes and may be an important modulator of this relational network. In this network, 11 miRNAs with a degree of two interacted with CSF1R, including hsa-miR-361-3p, hsa-miR-134-5p, and hsa-miR-218-5p (Fig. 3E). In addition, we also found that *NFE2L3* and *CSF1R* were the target genes of hsa-miR-361-3p related to diabetic wound healing in the miRNA-gene network (Fig. 3E).

2.4. Correlation analysis between the feature genes and immune infiltration

The correlation between the five feature genes and 13 infiltrating cells with relatively high infiltrating abundance was analyzed (Fig. 3F), and 12 gene–cell pairs with significant correlations were obtained (Table 1), including CORO1A–activated dendritic cells, CSF1R–activated dendritic cells, CSF1R–M1 macrophages, CSF1R–M2 macrophages, CTSH–activated dendritic cells, CTSH–M2 macrophages, CTSH– follicular helper T cells, NFE2L3–neutrophils, NFE2L3–CD8 T cells, SLC16A10–plasma cells, SLC16A10–follicular helper T cells, and SLC16A10–M2 macrophages (Fig. 3F).

2.5. Verification of the five feature genes and related miRNAs in the tissue and cell samples

The expression levels of the five feature genes were determined in nDFS and DFU tissue samples by qRT-PCR. Compared with the nDFS samples, the expression levels of *CORO1A*, *CSF1R*, *CTSH*, *NFE2L3*, and *SLC16A10* were significantly downregulated in the DFU samples ($P < 0.05$, Fig. 4A), and the expression level of *CSF1R* was the lowest in the DFU samples compared to that of the other four genes. Based on bioinformatics analysis, *CSF1R* was also closely related to M1 and M2 macrophages; therefore, *CSF1R* was selected for the subsequent experiments. According to the miRNA-gene network, miR-218-5p, miR-134-5p, and miR-361-3p interacted with *CSF1R*, and the levels of miR-218-5p were significantly decreased ($P < 0.05$), whereas miR-361-3p levels were significantly increased in the DFU samples compared with those in the nDFS samples ($P < 0.05$, Fig. 4B). No significant difference in miR-134-5p levels was found between nDFS and DFU samples (Fig. 4B). Therefore, *CSF1R*-miR-361-3p was selected for further experiments.

The expression levels of *CSF1R* and miR-361-3p were measured in AGE-treated RAW 264.7 cells. HSA treatment did not significantly affect the relative expression levels of *CSF1R* and miR-361-3p compared to those in the control group ($P > 0.05$, Fig. 4C, D, Figure S2). Relative to the control cells, the relative mRNA and protein expression of CSF1R was significantly downregulated in AGE-treated cells ($P < 0.05$, Fig. 4C, D, Figure S2), whereas the level of miR-361-3p was evidently higher in AGE-treated RAW 264.7 cells than in the control cells ($P < 0.05$, Fig. 4C). These results indicate that AGEs downregulate CSF1R expression while increasing miR-361-3p levels in RAW 264.7 cells.

Table 1
Information about a total of 12 gene -cell pairs with significant correlations.

gene	cell	r	p.value
CORO1A	Dendritic cells activated	−0.67948	0.000704
CSF1R	Dendritic cells activated	−0.77981	3.07E-05
CSF1R	Macrophages M2	0.535761	0.012307
CSF1R	Macrophages M1	0.507094	0.018964
CTSH	Dendritic cells activated	−0.55375	0.009204
CTSH	Macrophages M2	0.509753	0.018245
CTSH	T cells follicular helper	−0.45904	0.03633
NFE2L3	Neutrophils	−0.56756	0.007284
NFE2L3	T cells CD8	0.481564	0.02708
SLC16A10	Plasma cells	−0.45883	0.036424
SLC16A10	T cells follicular helper	−0.45384	0.038781
SLC16A10	Macrophages M2	0.443433	0.044069

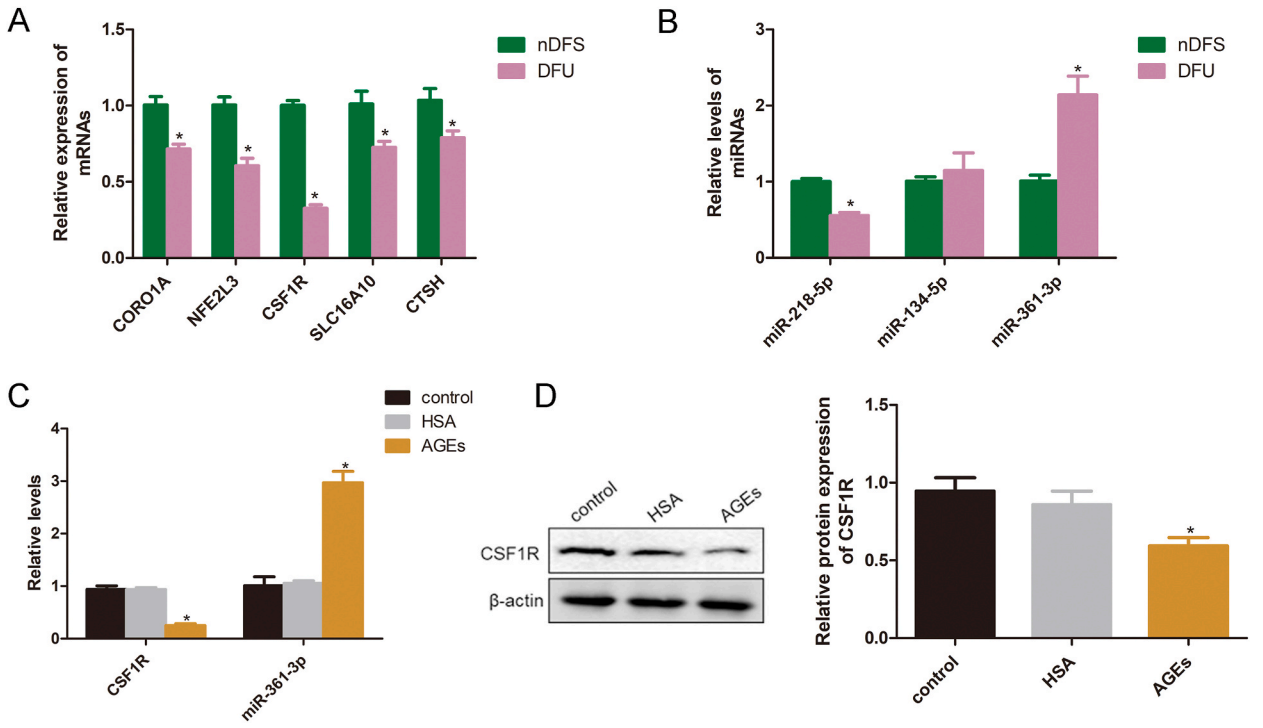

Fig. 4. Verification of the five feature genes and related miRNAs in the tissue and cell samples. (A) Expression levels of the five crucial feature genes in the clinical samples of DFU and nDFS using quantitative reverse transcription PCR (qRT-PCR). (B) Levels of miR-218-5p, miR-134-5p, and miR-361-3p in the clinical samples of DFU and nDFS using qRT-PCR. *$P < 0.05$, compared with the nDFS group. (C) Expression of *CSF1R* and miR-361-3p in the RAW 264.7 cells treated with AGEs using qRT-PCR. (D) Protein expression of CSF1R in the RAW 264.7 cells treated with AGEs using western blot. *$P < 0.05$, compared with the control cells.

2.6. MiR-361-3p inhibition reversed the apoptosis of RAW 264.7 cells induced by AGEs by PI3K-AKT pathway

To further explore the roles of miR-361-3p/*CSF1R* in AGE-induced RAW 264.7 cells, the cells with miR-361-3p inhibition or CSF1R knockdown were established. No significant differences in the expression levels of CSF1R and miR-361-3p were found between the AGEs and AGE + miR-361-3p NC groups ($P > 0.05$; Fig. 5A–C, Figure S3). Compared with the control group, the mRNA and protein expression of CSF1R was significantly downregulated in AGE-treated cells ($P < 0.05$); after miR-361-3p was inhibited, its expression was significantly upregulated compared with that in the AGE group ($P < 0.05$); whereas, after CSF1R knockdown, its expression was downregulated to a level similar to that in the AGE group ($P > 0.05$, Fig. 5A–C, Figure S3). The level of miR-361-3p was significantly increased in the AGE group relative to that in control cells ($P < 0.05$), and miR-361-3p inhibition decreased its level ($P < 0.05$, Fig. 5B).

The apoptosis of RAW 264.7 cells after different treatments was then determined. Compared to the control group, AGEs significantly enhanced the apoptosis of RAW 264.7 cells ($P < 0.05$), whereas miR-361-3p inhibition evidently decreased the cell apoptosis caused by AGEs ($P < 0.05$) and restored a similar level to that of the control cells ($P > 0.05$, Fig. 5D). However, si-CSF1R reversed the effects of the miR-361-3p inhibitor (Fig. 5D). Finally, the PI3K-AKT pathway was detected by western blotting. Compared to the control cells, the levels of p-AKT/AKT and p-PI3K/PI3K were significantly decreased in AGE-treated cells ($P < 0.05$). When miR-361-3p was inhibited in AGE-induced cells, the levels of p-AKT/AKT and p-PI3K/PI3K were significantly increased relative to those in the AGE group ($P < 0.05$); however, the levels caused by miR-361-3p inhibition could be reversed by *CSF1R* knockdown (Fig. 5E, Figure S4). These results suggest that miR-361-3p inhibition relieves the AGE-mediated apoptosis of RAW 264.7 cells by targeting *CSF1R* and activating the PI3K-AKT pathway.

2.7. Effects of miR-361-3p on wound healing process in diabetic mice

The effect of miR-361-3p on DFU wound healing was confirmed in a diabetic mouse model. After feeding mice with different treatments for 5, 10, and 15 days, miR-361-3p inhibition significantly promoted wound healing in diabetic mice compared to diabetic wound mice ($P < 0.05$), and the wounds healed on day 15, similar to the control group ($P > 0.05$, Fig. 6A and B). Additionally, the wound healing rate of mice gradually increased over time (Fig. 6B). The expression of CD68 in different groups was detected at the peak point (day 5) of the inflammatory response. The results showed that CD68 expression in diabetic wounded mice was significantly lower than that in control mice ($P < 0.05$), whereas miR-361-3p inhibition increased CD68 expression in diabetic wounded mice ($P < 0.05$; Fig. 6C), indicating that miR-361-3p inhibition may increase the number of macrophages in DFU mice. Finally, the protein

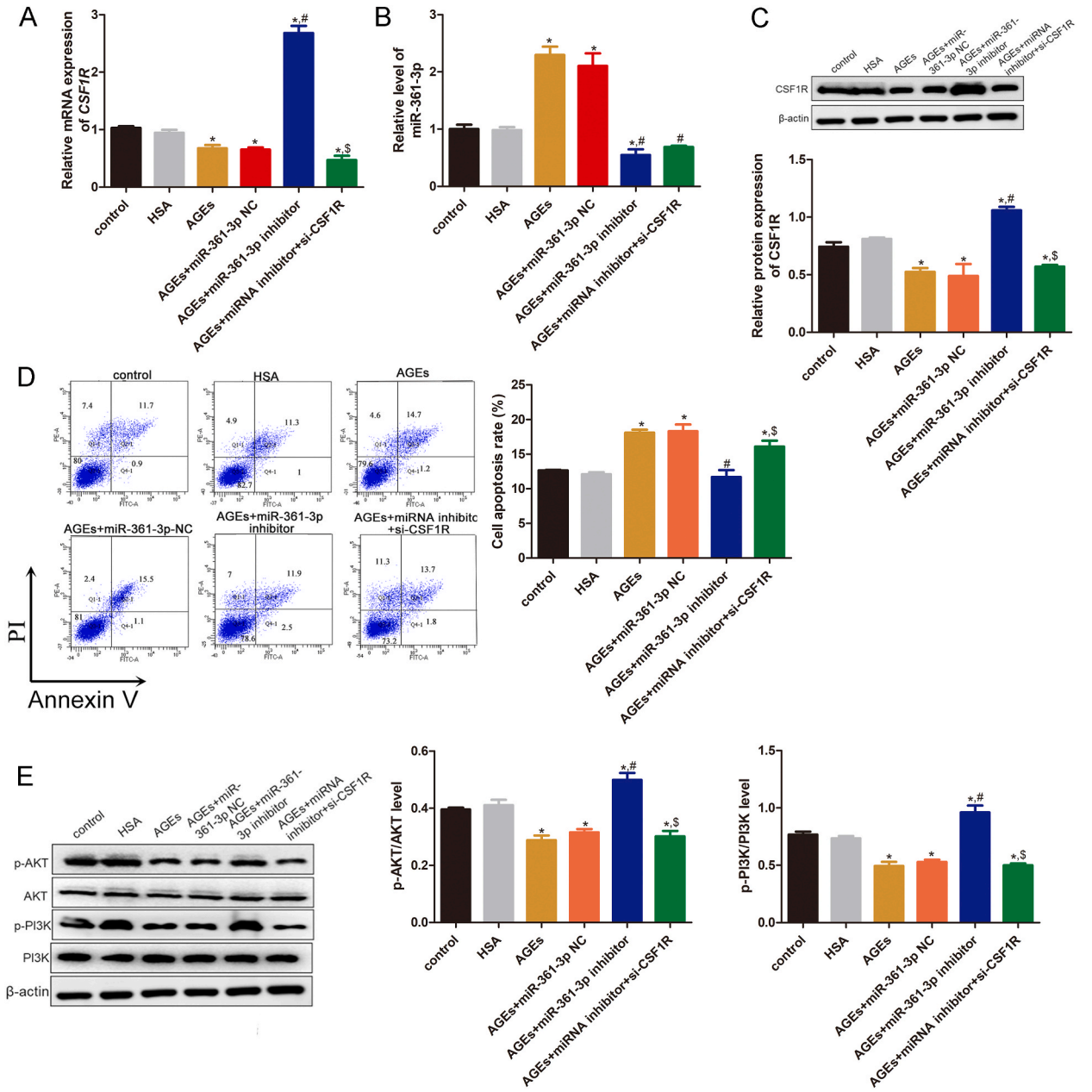

Fig. 5. MiR-361-3p inhibition reversed the apoptosis of RAW 264.7 cells induced by AGEs by PI3K-AKT pathway. (A) Expression of CSF1R in the cells transfected with miR-361-3p inhibitor or si-CSF1R using qRT-PCR. (B) Levels of miR-361-3p in the cells transfected with miR-361-3p inhibitor or si-CSF1R using qRT-PCR. (C) Protein expression of CSF1R in the cells transfected with miR-361-3p inhibitor or si-CSF1R by western blot. (D) Apoptosis of RAW 264.7 cells transfected with miR-361-3p inhibitor or si-CSF1R using flow cytometry. (E) Levels of p-PI3K/PI3K and p-AKT/AKT in the RAW 264.7 cells transfected with miR-361-3p inhibitor or si-CSF1R by western blot. $^{*}P < 0.05$, compared with the control group. $^{\#}P < 0.05$, compared with the AGE group. $^{\$}P < 0.05$, compared with the AGEs + miR-361-3p inhibitor group.

expression levels of CSF1R and PI3K/AKT were determined. It was found that CSF1R expression was significantly downregulated in diabetic wounded mice relative to control mice ($P < 0.05$), and miR-361-3p inhibition evidently upregulated its expression compared to that in diabetic mice ($P < 0.05$, Fig. 6D, E, Figure S5). In addition, the trends of p-AKT/AKT and p-PI3K/PI3K levels in the different groups were similar to those of CSF1R expression in the different groups (Fig. 6D, E, Figure S5).

3. Discussion

DFU is a common complication of diabetes and its management imposes a great financial burden on patients' families and medical

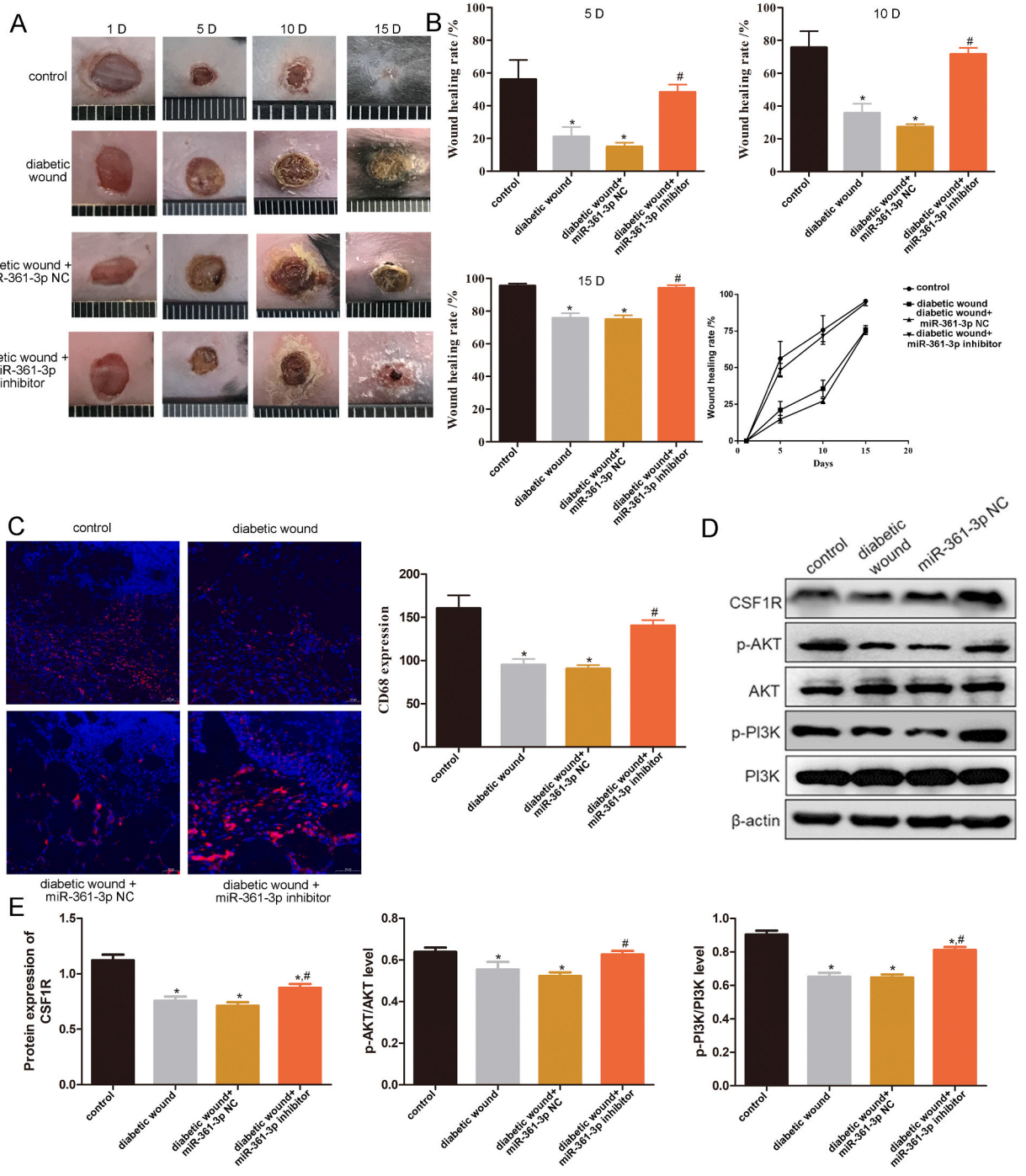

Fig. 6. Effects of miR-361-3p on wound healing process in diabetic mice. (A) Images of wound healing in diabetic mice after different treatments at 1, 5, 10, and 15 days. (B) Wound healing rate at 5, 10, and 15 days, and line chart of wound healing rate with the increasing time in the different groups. (C) Expression of CD68 in the different groups at the peak point (day 5) of the inflammatory response process by immunofluorescent staining. (D) Representative protein bands in the different groups. (E) Quantitative analysis of CSF1R, p-PI3K/PI3K, and p-AKT/AKT in the different groups. $^{*}P < 0.05$, compared with the control group. $^{\#}P < 0.05$, compared with the diabetic wound group.

systems. Macrophages play an important role in wound healing. Macrophage-free wounds can delay re-epithelialization, impair angiogenesis, reduce collagen deposition, and inhibit cell proliferation [20]. In patients with diabetes, the function of macrophages is altered, resulting in a weakened ability to clear infections and a delay in the repair process [21]. Yang et al. [22] demonstrated that dysregulation of macrophages may lead to impaired wound healing in patients with diabetes, and that hyaluronic acid-paeoniflorin

could promote diabetic wound healing by successfully achieving a paeoniflorin-mediated macrophage transition from M1 (pro-inflammatory) to M2 (anti-inflammatory and pro-healing). Our study showed that the number of macrophages decreased in DFU, which indicates their importance in this process. AGEs are formed by non-enzymatic reactions between proteins and glucose and can induce oxidative stress and inflammation in macrophages [23]. Our study found that AGEs inhibited cell viability while enhancing macrophage apoptosis. These results indicated that AGEs may be one of the reasons for poor wound healing through the regulation of macrophage growth in DFU patients [24]. Therefore, in additional cellular experiments, AGEs were employed to treat RAW 264.7 cells and mimic a DFU cellular model.

To further investigate the molecular mechanisms of DFU wound healing, bioinformatics analysis was performed, five crucial feature genes (*CORO1A*, *CSF1R*, *CTSH*, *NFE2L3*, and *SLC16A10*) were identified, and the combination of these five gens displayed high diagnostic value in DFU. Among these molecules, *CTSH* is a risk gene in type 1 diabetes, and transcriptional down-regulation of CTSH caused by pro-inflammatory cytokines could promote pancreatic β-cell apoptosis [25,26]. *CORO1A* plays a major role in integrin biology and controls neutrophil trafficking during innate immunity [27]. *SLC16A10* or *MCT10* participates in the transportation of extracellular aromatic amino acids [28]. Disruption of *SLC16A10* expression in NOD mice results in an increased incidence of type 1 diabetes [29]. *NFE2L3* (Nrf3) is a leucine zipper TF belonging to the Cap 'n' Collar family, which also includes Nrf2. Nrf2 activation promotes trauma repair in diabetic mice [30]. However, there is relatively little information on Nrf3. A recent study has revealed that Nrf3 facilitates ultraviolet radiation-related keratinocyte apoptosis by suppressing cell adhesion, indicating its potential role in wound healing [31]. *CSF1R* encodes a protein of the colony-stimulating factor receptor, which belongs to the platelet-derived growth factor receptor family [32]. It is broadly expressed on the surface of monocytes and macrophages. Taken together, we speculate that the combination of *CORO1A*, *CSF1R*, *CTSH*, *NFE2L3*, and *SLC16A10* may serve as a better diagnostic marker for predicting DFU.

Subsequently, the miRNAs and TFs upstream of these feature genes were predicted, and the expression of the five feature genes and their corresponding miRNAs was validated in clinical samples (DFU and nDFS). Eventually, the miR-361-3p–CSF1R pair with a significant negative correlation was selected for subsequent experiments. miR-361-3p has multiple biological functions and plays a key role in many diseases. Previous studies have demonstrated that miR-361-3p modulates cancer cell proliferation and migration by targeting several downstream genes, including *DUSP2* [33], *SOX9* [34], and *TGFB1* [35]. However, the specific pathogenic role of miR-361-3p in diabetic disease remains unclear. Huang et al. revealed that dysregulation of miR-361-3p is associated with hyperglycemia-mediated inflammation and apoptosis in vascular endothelial cells, leading to the pathophysiological manifestations of vascular complications in diabetes [36]. Additionally, a recent study [37] has reported that exosmic circRNAs from cancer cells interact with miR-361-3p to regulate M2 macrophage polarization and promote tumorigenesis. Considering the essential role of M2 macrophages in the wound healing process, the mechanism by which miR-361-3p affects macrophage polarization in DFU should be further verified.

CSF1R is the target gene of miR-361-3p, and binding of CSF1/CSF1R activates the PI3K-FOXO1 pathway and induces macrophage migration and M2 polarization [38]. CSF1R blockade inhibits the differentiation, proliferation, and survival of M2 macrophages and repolarizes tumor-associated macrophages towards the M1 type [39]. In our study, *CSF1R* was downregulated in AGE-treated macrophages, whereas miR-361-3p levels were increased. Additionally, both *in vitro* and *in vivo* experiments showed that miR-361-3p inhibition attenuated AGE-mediated apoptosis of RAW 264.7, and increased CSF1R expression and p-AKT/AKT and p-PI3K/PI3K levels. PI3K/AKT has been reported as a classic signaling pathway in cells that plays an active role in wound repair; activated AKT signaling can directly affect the survival, polarization, and migration of macrophages [40,41]. Combined with our findings, it can be inferred that miR-361-3p suppression may inhibit AGE-induced macrophage apoptosis by targeting *CSF1R* and activating the PI3K/AKT pathway.

However, this study has several limitations. First, additional clinical cases and studies are required to clarify the molecular mechanisms of miR-361-3p/CSF1R. Second, miR-361-3p may exert its effects through other downstream genes. Moreover, the potential functions of other feature genes or interacting miRNAs in diabetic wound healing need to be investigated and verified through experimental assays.

4. Conclusion

In conclusion, this study identified five crucial feature genes (*CORO1A*, *CSF1R*, *CTSH*, *NFE2L3*, and *SLC16A10*) and their corresponding miRNAs by analyzing the transcriptional profiles of DFU samples. The combination of these five feature genes may provide a better diagnostic model for DFU patient prediction. Additionally, AGEs may regulate macrophage apoptosis via the miR-361-3p/CSF1R axis and PI3K/AKT pathway, thereby influencing DFU wound healing. This study improves our understanding of macrophage apoptosis in the wound healing process of DFU and provides a basis for determining the miR-361-3p/CSF1R axis and PI3K/AKT pathway as novel therapeutic targets and pathways to promote wound healing in DFU.

5. Materials and methods

5.1. Patient demographics

DFU and nDFS tissue samples (acute wound amputation specimens) were collected from clinical patients in the Department of General Surgery of Putuo Hospital, Shanghai University of Traditional Chinese Medicine (Shanghai, China). The inclusion and exclusion criteria for DFU have been previously described [42]. Tissue samples were preserved in RNAlater for RNA extraction or fixed in paraformaldehyde for immunofluorescence detection. This study was approved by the Ethics Committee of Putuo District Center

Hospital, Shanghai (Putuo Hospital, Shanghai University of Traditional Chinese Medicine, approval No: PTEC-R-2021-13-1, date: 2021-04-30). Informed consent was obtained from all the patients.

5.2. Data resources and preprocess

Microarray data were downloaded from the GEO database of the NCBI for Biotechnology Information (https://www.ncbi.nlm.nih.gov/). The GSE134431 dataset [43] comprises RNA-seq profiles from patients with DFU, including eight nDFS samples, seven DFU healer samples, and six DFU non-healer samples. All the data were tested on the platform of Illumina NextSeq 500 (*Homo sapiens*). The GSE97615 dataset [44] includes the expression profiles of human oral and cutaneous wound tissue samples. We selected 12 skin wound healing samples for further analysis at three time points: days 1, 3, and 6 (four samples per time point). The dataset was tested using the Illumina HiSeq 2000 platform (*Homo sapiens*). After quality control, alignment, and quantitative analysis, the RPKM expression matrix was obtained from the database and $\log_2$ transformed (RPKM+1) for downstream analysis.

5.3. Screening differentially expressed genes (DEGs)

The Limma package version 3.34.7 [45] in R3.6.1 (https://bioconductor.org/packages/release/bioc/html/limma.html) was used to identify DEGs related to DFU. For the GSE134431 dataset, pairwise comparisons were performed between the nDFS, DFU healer, and DFU non-healer groups. For the GSE97615 dataset, pairwise comparisons were performed at each time point. P value < 0.05 and $|\log_2$fold change (FC)$| > 1$ were selected as thresholds to screen DEGs. After pairwise comparison of the two groups, DEGs were obtained and combined into a union cohort. Then, time-series clustering analysis were conducted using the Mfuzz package [46] version 2.42.0 (http://bioconductor.org/packages/release/bioc/html/Mfuzz.html) to analyze gene expression in each group. The parameter was set as a member. Ship = 0.3.

5.4. Functional enrichment analysis and protein–protein interaction (PPI) network

GO and KEGG (approved by Kanehisa Laboratories, Kyoto, Japan) enrichment analyses of the identified DEGs were conducted using the DAVID [47] tool (Version 6.8, https://david-d.ncifcrf.gov/). $P < 0.05$, and count number >2 were considered significantly enriched terms.

The STRING [48] (Version: 10.0, http://www.string-db.org/) database was used to predict protein interactions in *Homo sapiens*. The PPI score was set as 0.4 (medium confidence). Cytoscape software [49] (version 3.4.0; http://chianti.ucsd.edu/cytoscape-3.4.0/) was used to construct the PPI network.

5.5. Screening and validation of crucial genes

LASSO Cox regression analysis was performed using the Glmnet package [50] version 4.0-2 (https://cran.r-project.org/web/packages/glmnet/index.html) to identify optimal feature genes. Selected genes were evaluated using a 20 fold cross-validation process (nfold = 20). Here, we mainly focused on the differences between the unhealed, healed, and normal groups; thus, the healed and normal samples were integrated into one group. Next, the expression values of the selected genes were extracted from the GSE134431 dataset and eigenvalues were calculated using the following formula:

$$feature_{sample} = \sum_{1}^{n} Coef_i * x_i$$

here, $Coef_i$ represents the LASSO regression coefficient of the "i-th" gene; x_i represents the expression value of the "i-th" gene, whereas n represents the gene counts. Based on this formula, we obtained the eigenvalues for each sample. An ROC curve was generated using the pROC package to evaluate the predictive ability of selected genes.

5.6. Predicting upstream transcription factors (TFs) of feature genes

The iRegulon plugin [51] (Version 1.3, http://iregulon.aertslab.org/) was used to predict the upstream TFs of feature genes. The parameters were set as follows: 10 K motif collections (9713 PWMs) and 1120 ChIP-seq track collections (minimum nescore = 3, rank threshold for visualization = 5000). The TFs with more than three target genes were selected to construct a regulatory network.

Six databases, miRWalk, miRanda, microt4, RNA22, TargetScan, and PITA, were used to predict the corresponding miRNAs of the feature genes using Mirwalk2.0 [52] (http://zmf.umm.uni-heidelberg.de/apps/zmf/mirwalk2/) tools. miRNA–mRNA pairs that existed in more than four databases were selected as candidate pairs to generate miRNA–mRNA networks.

5.7. Correlation analysis between the feature genes expression and immune cell infiltration

The CIBERSORT tool [53] was employed to detect the abundance of 22 immune cells in each sample. The correlation between feature genes and immune-infiltrating cells was evaluated using Spearman's coefficient (cor function, http://77.66.12.57/R-help/cor.test.html).

5.8. Wound healing assay in diabetic mice model

All animal experiments were conducted in accordance with the ARRIVE guidelines (https://arriveguidelines.org/) and approved by the Animal Experimental Ethics Committee of Ruijin Hospital, Shanghai Jiao Tong University School of Medicine (date: 2018-11-16). Twenty-four male type 2 diabetic db/db mice (7–9 weeks old) were purchased from Shanghai Slack Laboratory Animal Co., Ltd. All the mice were monitored for blood glucose and weight, with diabetes status defined as blood glucose >200 mg/dl. Mice that lost more than 20% of their body weight were excluded from the experiments. A total of 24 mice were selected and divided into four groups (n = 6): control, diabetic wounds, diabetic wounds + miR-361-3p NC, and diabetic wounds + miR-361-3p inhibitor. Mice with diabetic wounds were established as previously described [42]. Briefly, mice were anesthetized with 4% isoflurane. The skin on the back was shaved and wiped with 70% ethanol. Two skin wounds of 2 mm were created on the back side using a 6 mm full-thickness sterile biopsy punch and sterilized with 75% ethanol. Mice in the diabetic wound, diabetic wound + miR-361-3p NC, and diabetic wound + miR-361-3p inhibitor groups were first established as diabetic wounds, and then mice in the diabetic wound + miR-361-3p NC and diabetic wound + miR-361-3p inhibitor groups were treated with miR-361-3p NC or inhibitor every 2 days for 6 days. The wound healing process was assessed using ImageJ software at the indicated time points (days 1, 5, 10, and 15).

5.9. Immunofluorescence staining

Patient tissues or wound-edge skin tissues from mice were fixed in 4% paraformaldehyde solution and dehydrated in an ethanol gradient. After clearing with xylene, tissue samples were embedded in paraffin and cut into histological sections (RM2016, Shanghai Leica Instrument Co., Ltd. Shanghai, China). The slides were then incubated with a primary antibody (CD68; Affinity, USA), followed by incubation with a goat anti-rabbit secondary antibody. Images were obtained using a confocal microscope (Nikon C1 Eclipse; Nikon).

5.10. Cell transfection assay

RAW 264.7 cells were cultured in DMEM (Gibco, USA) supplemented with 10% fetal bovine serum (Gibco, USA) and penicillin–streptomycin (100 U/mL). miR-361-3p inhibitor/NC and si-CSF1R were obtained from Shanghai Genomeditech, Inc. (Shanghai, China). Cell transfection was performed using Lipofectamine 2000 (Thermo Fisher Scientific) following the manufacturer's protocol. Briefly, the cells were treated with extrinsic AGEs (Sunteambio, CHINA), and then transfected with miR-361-3p inhibitor/NC and si-CSF1R. After transfected for 6 h, the serum-free medium was replaced with complete medium and the cells were cultured for another 48 h. Total RNA was extracted from cells subjected to different treatments, and cell transfection efficiency was evaluated by determining the levels of miR-361-3p and CSF1R using quantitative reverse transcription PCR (RT-qPCR) and western blotting.

5.11. Cell viability and apoptosis assays

The cells with different treatments were harvested, and a cell counting kit-8 (CCK8, Biosharp, Wuhan, China) was used to assess the effects of AGEs on the growth of RAW 264.7 cells. Briefly, the cells were added with 10 μL CCK8 reagent, and incubated for 2.5 h. The optical density (OD) at 450 nm was measured using an Infinite 200Pro (Tecan, Mannedorf, Switzerland).

Annexin V/PI dual staining (BestBio, Shanghai, China) was used to detect the apoptosis rate of the macrophages. The cells with different treatments were collected, and AnnexinV-FITC (5 μL) and PI (10 μL) were added to 400 μL cell suspension. After incubation in the dark for 15 min, cell acquisition was conducted using an Attune CytPix flow cytometer (Thermo, CA, USA), and data were analyzed using FlowJo software. Each experiment was performed in triplicate.

Table 2
The sequences of all primers.

Genes/miRNAs	Forward primer (5′-3′)	Reverse primer (5′-3′)
hsa-miR-134-5p	CGCGTGTGACTGGTTGACCA	GTCGTATCCAGTGCAGGGTCCGAGGTATTCGCACTGGATACGACCCCCTC
hsa-miR-218-5p	GCGCGTTGTGCTTGATCTAA	GTCGTATCCAGTGCAGGGTCCGAGGTATTCGCACTGGATACGACACATGG
muu-miR-361-3p	TCCCCCAGGTGTGATTCTG	GTCGTATCCAGTGCAGGGTCCGAGGTATTCGCACTGGATACGACACAAAT
hsa-miR361-3p	CGTCCCCCAGGTGTGATTC	GTCGTATCCAGTGCAGGGTCCGAGGTATTCGCACTGGATACGACAAATCA
hsa-CORO1A	GGCTTTTGGGGGATCACTGT	CGAAGAGGCTGCTAGGTCG
mus-CORO1A	GTGTCCCCTTCCTGTCTTGG	GGAATTTGCTGGAGCGAACC
hsa-CSF1R	ATCAGCCCAAGGAGGAGGAA	CAGCAGGAGCAGCAGAACT
mus-CSF1R	TGGCGAGGGTTCATTATCCG	CCAGCTTGCTAGGCTCCAAT
hsa-CTSH	AGAGCTCCAGGGACTGTCTT	GGTGGATAATACCGCCAGCA
mus-CTSH	AAGCCCACAACCAGAGGAAC	TCCATGGAGGAAGGGTAGGG
hsa-NFE2L3	GGAGGGCATCTCATTGGGAG	GGGACAAAGCAAGATGGCCT
mus-NFE2L3	GCTGTGGATCACAGTTCCCA	CAGAGGCACACGCCATTTTG
hsa-SLC16A10	AGGCCCTGGGCTCACTATAA	CTTAACTGCGAGCATTCGGC
mus-SLC16A10	TGATGAACATGGCCTCCCAA	GAGCTCCCTACCTCTATGCC
U6	CTCGCTTCGGCAGCACA	AACGCTTCACGAATTTGCGT

5.12. Quantitative reverse transcription PCR (qRT-PCR)

Total RNA was extracted from the skin tissue or cells using the RNAiso Plus kit (Trizol, Takara Biomedical Technology Co., Ltd., Beijing, China). Then, a miR-X miRNA first-Strand synthesis kit (Clontech, CA, USA) was used for the cDNA synthesis, and miRNA qRT-PCR TB Green®Kit (Clontech, CA, USA) was used for RT-PCR analysis. The sequences of all primers are listed in Table 2. qPCR was performed using an ABI7500 RT-PCR System (Thermo, Massachusetts, USA). The relative expression levels of miRNAs and mRNAs were analyzed based on the $2^{-\Delta\Delta Ct}$ method.

5.13. Western blotting

RIPA lysis buffer was used to extract the total protein. Protein samples were separated using SDS-PAGE, transferred onto PVDF membranes, and blocked with 5% skim milk. The membranes were incubated with primary antibodies, followed by secondary antibodies. The primary antibodies used in this study were listed as follows: CSF1R (Affinity, USA); PI3K p85β phospho Tyr464 (Immunoway, TX, USA), PI3k p85α (Abcam, Cambridge, UK), Akt (CST, MA, USA), and pAkt-Ser473 (CST, MA, USA). The expression levels of the related proteins were detected using an ECL kit and visualized using Image Quant LAS 4000 mini (GE Healthcare, USA).

5.14. Statistical analysis

Data from three independent experiments were shown as mean ± standard deviation (SD). Statistical analyses were performed using GraphPad Prism 8.0 (GraphPad Software, San Diego, CA, USA). For two-group analyses, Student's *t*-test was used, while one-way ANOVA followed by Tukey's post hoc test was performed for more than two-group analyses. $P < 0.05$ was considered statistically significant.

Ethics approval and consent to participate

This study was approved by the Ethics Committee of the Ethics Committee of Putuo District Center Hospital, Shanghai (Putuo Hospital, Shanghai University of Traditional Chinese Medicine, approval No: PTEC-R-2021-13-1, date: 2021-04-30), and the Animal Experimental Ethics Committee of Ruijin Hospital, Shanghai Jiao Tong University School of Medicine (date: 2018-11-16). Informed consent was obtained from all the patients. All methods were reported in accordance with the ARRIVE guidelines (https://arriveguidelines.org) for animal experiments.

Consent for publication

Not applicable.

Data availability

The data used to support the findings of this study are available from the GEO (https://www.ncbi.nlm.nih.gov/) database under the accession number GSE134431(https://www.ncbi.nlm.nih.gov/geo/query/acc.cgi?acc=GSE134431) and GSE97615 (https://www.ncbi.nlm.nih.gov/geo/query/acc.cgi?acc=GSE97615). Additionally, other data used and/or analyzed in the current study are available from the corresponding author upon reasonable request.

Funding

This study was supported by the Special Disease Construction Project of Putuo District (No. 2020tszb01), Shanghai Putuo District Health System Science and Technology Innovation Project (No. ptkwws202312), and the National Natural Science Foundation of China (No. 81670752).

CRediT authorship contribution statement

Yongzhi Jin: Writing – original draft, Methodology, Investigation, Conceptualization. **Yi Huang:** Resources, Methodology, Investigation, Data curation. **Guang Zeng:** Investigation, Formal analysis, Data curation. **Junsheng Hu:** Validation, Resources, Methodology, Investigation. **Mengfan Li:** Validation, Methodology, Investigation, Formal analysis. **Ming Tian:** Writing – review & editing, Visualization, Supervision, Funding acquisition, Conceptualization. **Tao Lei:** Writing – review & editing, Supervision, Funding acquisition, Conceptualization. **Rong Huang:** Writing – review & editing, Project administration, Funding acquisition, Conceptualization.

Declaration of competing interest

The authors declare that they have no known competing financial interests or personal relationships that could have appeared to influence the work reported in this paper.

Acknowledgements

None.

Abbreviations

AGEs	advanced glycosylation end products
DFU	diabetic foot ulcer
GO	Gene Ontology
KEGG	Kyoto Encyclopedia of Genes and Genomes
LASSO	least absolute shrinkage and selection operator
nDFS	non-diabetic foot skin
TFs	transcription factor

Appendix A. Supplementary data

Supplementary data to this article can be found online at https://doi.org/10.1016/j.heliyon.2024.e24598.

References

[1] P. Zhang, J. Lu, Y. Jing, S. Tang, D. Zhu, Y. Bi, Global epidemiology of diabetic foot ulceration: a systematic review and meta-analysis (†), Ann. Med. 49 (2017) 106–116.
[2] D.G. Armstrong, A.J.M. Boulton, S.A. Bus, Diabetic foot ulcers and their recurrence, N. Engl. J. Med. 376 (2017) 2367–2375.
[3] X. Chen, W. Zhou, K. Zha, G. Liu, S. Yang, S. Ye, et al., Treatment of chronic ulcer in diabetic rats with self assembling nanofiber gel encapsulated-polydeoxyribonucleotide, Am. J. Transl. Res. 8 (2016) 3067–3076.
[4] T. He, P. Sun, B. Liu, S. Wan, P. Fang, J. Chen, et al., Puffball spores improve wound healing in a diabetic rat model, Front. Endocrinol. 13 (2022) 942549.
[5] X. Liu, G. Dou, Z. Li, X. Wang, R. Jin, Y. Liu, et al., Hybrid biomaterial initiates refractory wound healing via inducing transiently heightened inflammatory responses, Adv. Sci. 9 (2022) e2105650.
[6] S.Y. Kim, M.G. Nair, Macrophages in wound healing: activation and plasticity, Immunol. Cell Biol. 97 (2019) 258–267.
[7] E. Santos-Vizcaino, A. Salvador, C. Vairo, M. Igartua, R.M. Hernandez, L. Correa, et al., Overcoming the inflammatory stage of non-healing wounds: in vitro mechanism of action of negatively charged microspheres (NCMs), Nanomaterials 10 (2020) 1108.
[8] S. Nassiri, I. Zakeri, M.S. Weingarten, K.L. Spiller, Relative expression of proinflammatory and antiinflammatory genes reveals differences between healing and nonhealing human chronic diabetic foot ulcers, J. Invest. Dermatol. 135 (6) (2015 Jun) 1700–1703, https://doi.org/10.1038/jid.2015.30. Epub 2015 Feb 3.
[9] M.Y. Zeng, D. Pham, J. Bagaitkar, J. Liu, K. Otero, M. Shan, et al., An efferocytosis-induced, IL-4-dependent macrophage-iNKT cell circuit suppresses sterile inflammation and is defective in murine CGD, Blood 121 (2013) 3473–3483.
[10] S. Khanna, S. Biswas, Y. Shang, E. Collard, A. Azad, C. Kauh, et al., Macrophage dysfunction impairs resolution of inflammation in the wounds of diabetic mice, PLoS One 5 (2010) e9539-e.
[11] K. Das, L.V.M. Rao, The role of microRNAs in inflammation, Int. J. Mol. Sci. 23 (2022).
[12] W. Wang, C. Yang, X.Y. Wang, L.Y. Zhou, G.J. Lao, D. Liu, et al., MicroRNA-129 and -335 promote diabetic wound healing by inhibiting sp1-mediated MMP-9 expression, Diabetes 67 (2018) 1627–1638.
[13] H. Wang, X. Wang, X. Liu, J. Zhou, Q. Yang, B. Chai, et al., miR-199a-5p plays a pivotal role on wound healing via suppressing VEGFA and ROCK1 in diabetic ulcer foot, Oxid. Med. Cell. Longev. 7 (2022).
[14] P. Wang, G. Theocharidis, I.S. Vlachos, K. Kounas, A. Lobao, B. Shu, et al., Exosomes derived from epidermal stem cells improve diabetic wound healing, J. Invest. Dermatol. 16 (2022), 00119-1.
[15] D. Zhang, Y. Wu, Z. Li, H. Chen, S. Huang, C. Jian, et al., MiR-144-5p, an exosomal miRNA from bone marrow-derived macrophage in type 2 diabetes, impairs bone fracture healing via targeting Smad1, J. Nanobiotechnol. 19 (2021) 226.
[16] M. Teng, Z. Li, X. Wu, Z. Zhang, Z. Lu, K. Wu, et al., Development of tannin-bridged cerium oxide microcubes-chitosan cryogel as a multifunctional wound dressing, Colloids Surf. B Biointerfaces 214 (2022) 112479.
[17] Y. Xing, S. Pan, L. Zhu, Q. Cui, Z. Tang, Z. Liu, et al., Advanced glycation end products induce atherosclerosis via RAGE/TLR4 signaling mediated-M1 macrophage polarization-dependent vascular smooth muscle cell phenotypic conversion, Oxid. Med. Cell. Longev. 2022 (2022) 9763377.
[18] S. He, Q. Hu, X. Xu, Y. Niu, Y. Chen, Y. Lu, et al., Advanced glycation end products enhance M1 macrophage polarization by activating the MAPK pathway, Biochem. Biophys. Res. Commun. 525 (2020) 334–340.
[19] Y. Rong, H. Yang, H. Xu, S. Li, P. Wang, Z. Wang, et al., Bioinformatic analysis reveals hub immune-related genes of diabetic foot ulcers, Front. Surg. 9 (2022).
[20] R. Mirza, L.A. DiPietro, T.J. Koh, Selective and specific macrophage ablation is detrimental to wound healing in mice, Am. J. Pathol. 175 (2009) 2454–2462.
[21] S.M. Aitcheson, F.D. Frentiu, S.E. Hurn, K. Edwards, R.Z. Murray, Skin wound healing: normal macrophage function and macrophage dysfunction in diabetic wounds, Molecules 26 (2021).
[22] H. Yang, L. Song, B. Sun, D. Chu, L. Yang, M. Li, et al., Modulation of macrophages by a paeoniflorin-loaded hyaluronic acid-based hydrogel promotes diabetic wound healing, Mater. Today Bio. 12 (2021) 100139.
[23] J. Teng, Y. Li, W. Yu, Y. Zhao, X. Hu, N.P. Tao, et al., Naringenin, a common flavanone, inhibits the formation of AGEs in bread and attenuates AGEs-induced oxidative stress and inflammation in RAW264.7 cells, Food Chem. 269 (2018) 35–42.
[24] L. Van Putte, S. De Schrijver, P. Moortgat, The effects of advanced glycation end products (AGEs) on dermal wound healing and scar formation: a systematic review, Scar. Burn. Heal. 2 (2016) 2059513116676828.
[25] T. Fløyel, C. Brorsson, L.B. Nielsen, M. Miani, C.H. Bang-Berthelsen, M. Friedrichsen, et al., CTSH regulates β-cell function and disease progression in newly diagnosed type 1 diabetes patients, Proc. Natl. Acad. Sci. U.S.A. 111 (2014) 10305–10310.
[26] J. Ye, M. Stefan-Lifshitz, Y. Tomer, Genetic and environmental factors regulate the type 1 diabetes gene CTSH via differential DNA methylation, J. Biol. Chem. 296 (2021) 14.
[27] R. Pick, D. Begandt, T.J. Stocker, M. Salvermoser, S. Thome, R.T. Böttcher, et al., Coronin 1A, a novel player in integrin biology, controls neutrophil trafficking in innate immunity, Blood 130 (2017) 847–858.
[28] L. Mariotta, T. Ramadan, D. Singer, A. Guetg, B. Herzog, C. Stoeger, et al., T-type amino acid transporter TAT1 (Slc16a10) is essential for extracellular aromatic amino acid homeostasis control, J. Physiol. 590 (2012) 6413–6424.

[29] C.M. Elso, E.P.F. Chu, M.A. Alsayb, L. Mackin, S.T. Ivory, M.P. Ashton, et al., Sleeping beauty transposon mutagenesis as a tool for gene discovery in the NOD mouse model of type 1 diabetes, G3 (Bethesda) 5 (2015) 2903–2911.
[30] M. Long, M. Rojo de la Vega, Q. Wen, M. Bharara, T. Jiang, R. Zhang, et al., An essential role of NRF2 in diabetic wound healing, Diabetes 65 (2016) 780–793.
[31] B. Siegenthaler, C. Defila, S. Muzumdar, H.-D. Beer, M. Meyer, S. Tanner, et al., Nrf3 promotes UV-induced keratinocyte apoptosis through suppression of cell adhesion, Cell Death Differ. 25 (2018) 1749–1765.
[32] P.S. Tripathy, N.C. Devi, J. Parhi, H. Priyadarshi, A.B. Patel, P.K. Pandey, et al., Molecular mechanisms of natural carotenoid-based pigmentation of queen loach, Botia dario (Hamilton, 1822) under captive condition, Sci. Rep. 9 (2019) 12585.
[33] Y. Qin, J. Ye, F. Zhao, S. Hu, S. Wang, TRIM2 regulates the development and metastasis of tumorous cells of osteosarcoma, Int. J. Oncol. 53 (2018) 1643–1656.
[34] S. He, Y. Feng, W. Zou, J. Wang, G. Li, W. Xiong, et al., The role of the SOX9/lncRNA ANXA2P2/miR-361-3p/SOX9 regulatory loop in cervical cancer cell growth and resistance to cisplatin, Front. Oncol. (2022) 11.
[35] Y. Zhou, Q. Zhang, B. Liao, X. Qiu, S. Hu, Q. Xu, circ_0006089 promotes gastric cancer growth, metastasis, glycolysis, and angiogenesis by regulating miR-361-3p/TGFB1, Cancer Sci. 29 (2022) 15351.
[36] K. Huang, X. Yu, Y. Yu, L. Zhang, Y. Cen, J. Chu, Long noncoding RNA MALAT1 promotes high glucose-induced inflammation and apoptosis of vascular endothelial cells by regulating miR-361-3p/SOCS3 axis, Int. J. Clin. Exp. Pathol. 13 (2020) 1243–1252.
[37] C. Lu, W. Shi, W. Hu, Y. Zhao, X. Zhao, F. Dong, et al., Endoplasmic reticulum stress promotes breast cancer cells to release exosomes circ_0001142 and induces M2 polarization of macrophages to regulate tumor progression, Pharmacol. Res. 177 (2022) 26.
[38] Y. Zhou, J. Zeng, Y. Tu, L. Li, S. Du, L. Zhu, et al., CSF1/CSF1R-mediated crosstalk between choroidal vascular endothelial cells and macrophages promotes choroidal neovascularization, Invest. Ophthalmol. Vis. Sci. 62 (2021) 37.
[39] Q. Wang, Y. Lu, R. Li, Y. Jiang, Y. Zheng, J. Qian, et al., Therapeutic effects of CSF1R-blocking antibodies in multiple myeloma, Leukemia 32 (2018) 176–183.
[40] M.F. Linton, J.J. Moslehi, V.R. Babaev, Akt signaling in macrophage polarization, survival, and atherosclerosis, Int. J. Mol. Sci. 20 (2019) 2703.
[41] S.W. Jere, N.N. Houreld, H. Abrahamse, Role of the PI3K/AKT (mTOR and GSK3β) signalling pathway and photobiomodulation in diabetic wound healing, Cytokine Growth Factor Rev. 50 (2019) 52–59.
[42] A.P. Sawaya, R.C. Stone, S.R. Brooks, I. Pastar, I. Jozic, K. Hasneen, et al., Deregulated immune cell recruitment orchestrated by FOXM1 impairs human diabetic wound healing, Nat. Commun. 11 (2020) 4678.
[43] M.-S. Gan, B. Yang, D.-L. Fang, B.-L. Wu, IL-1B can serve as a healing process and is a critical regulator of diabetic foot ulcer, Ann. Transl. Med. 10 (2022) 179.
[44] R. Iglesias-Bartolome, A. Uchiyama, A.A. Molinolo, L. Abusleme, S.R. Brooks, J.L. Callejas-Valera, et al., Transcriptional signature primes human oral mucosa for rapid wound healing, Sci. Transl. Med. 10 (2018).
[45] M.E. Ritchie, B. Phipson, D. Wu, Y. Hu, C.W. Law, W. Shi, et al., Limma powers differential expression analyses for RNA-sequencing and microarray studies, Nucleic Acids Res. 43 (2015) 20.
[46] L. Kumar, M EF. Mfuzz: a software package for soft clustering of microarray data, Bioinformation 2 (2007) 5–7.
[47] da W. Huang, B.T. Sherman, R.A. Lempicki, Systematic and integrative analysis of large gene lists using DAVID bioinformatics resources, Nat. Protoc. 4 (2009) 44–57.
[48] D. Szklarczyk, J.H. Morris, H. Cook, M. Kuhn, S. Wyder, M. Simonovic, et al., The STRING database in 2017: quality-controlled protein-protein association networks, made broadly accessible, Nucleic Acids Res. 45 (2017) D362–D368.
[49] P. Shannon, A. Markiel, O. Ozier, N.S. Baliga, J.T. Wang, D. Ramage, et al., Cytoscape: a software environment for integrated models of biomolecular interaction networks, Genome Res. 13 (2003) 2498–2504.
[50] X.N. Bui, H. Nguyen, Q.H. Tran, H.B. Bui, Q.L. Nguyen, D.A. Nguyen, et al., A lasso and elastic-net regularized generalized linear model for predicting blast-induced air over-pressure in open-pit mines, Inżynieria Mineralna. 21 (2019).
[51] A. Verfaillie, H. Imrichova, R. Janky, S. Aerts, iRegulon and i-cisTarget: reconstructing regulatory networks using motif and track enrichment, Curr. Protoc. Bioinform. 52 (2015) 1–2.
[52] H. Dweep, N. Gretz, miRWalk2.0: a comprehensive atlas of microRNA-target interactions, Nat. Methods 12 (8) (2015 Aug) 697, https://doi.org/10.1038/nmeth.3485.
[53] B. Chen, M.S. Khodadoust, C.L. Liu, A.M. Newman, A.A. Alizadeh, Profiling tumor infiltrating immune cells with CIBERSORT, Methods Mol. Biol. (2018) 7493, 1_12.